Tungsten (2019) 1:287–296
https://doi.org/10.1007/s42864-019-00029-2

Tungsten
www.springer.com/42864

ORIGINAL PAPER

Active La–Nb–O compounds for fast lithium-ion energy storage

Kunfeng Chen[1] · Shu Yin[2] · Dongfeng Xue[1]

Received: 7 August 2019 / Revised: 26 September 2019 / Accepted: 9 October 2019 / Published online: 17 December 2019

Abstract
Searching for novel complex materials with enhanced lithium-ion battery performances is one of the most challenging efforts. Many kinds of transition metal oxides and polyanionic frameworks were developed with various structures, which can improve the energy density of lithium-ion batteries. In this work, we explored 4d and 4f transition metal La–Nb–O compounds as cathode materials for lithium-ion energy storage. Orthorhombic pyrochlore $LaNb_5O_{14}$, orthorhombic perovskite $LaNb_3O_9$, and monoclinic $LaNbO_4$ compounds with different metal cation coordination polyhedra were synthesized using solid-state reaction. The orthorhombic pyrochlore $LaNb_5O_{14}$ compound showed the highest capacity among these La–Nb–O compounds owing to its quasi-2D network for Li-ion incorporation. According to the electronegativity theory and ionic size, La^{3+} cations can form LaO_{12} polyhedra and hexahedral LaO_8 units in different La–Nb–O compounds, which can stabilize octahedral NbO_6 and/or pentahedral NbO_7 and their assembled structures, resulting in easy lithium-ion diffusion. This work may provide some structure clues for the design of electrode materials for fast lithium storage.

Keywords Lanthanum orthoniobates · Pyrochlore · Perovskite · Multiple cation materials · Lithium-ion battery

1 Introduction

The design and synthesis of transition metal compounds with targeted properties and enhanced performances is important to develop the present and future technologies [1]. For fast energy storage applications, novel electrode materials are urgent to enhance both their capacities and charge storage kinetics [2, 3]. Recently, two novel complex niobium tungsten oxides ($Nb_{16}W_5O_{55}$ and $Nb_{18}W_{16}O_{93}$) were synthesized to effectively use superstructure motifs to provide stable host structures for lithium intercalation with facile and defect-tolerant lithium diffusion and multi-electron redox [4]. At a current density of 20 C, the $Nb_{18}W_{16}O_{93}$ material shows a capacity of ~ 150 mAh g^{-1}. Even at a current density of 60 C (8.9 A g^{-1}) and 100 C (14.9 A g^{-1}), the capacities are 105 and 70 mAh g^{-1}, respectively. For fast lithium-ion energy storage, nanostructured materials, e.g., TiO_2, $Li_4Ti_5O_{12}$, and Nb_2O_5, were proved to overcome poor ionic diffusion and electronic properties [5–7]. Among these materials, orthorhombic Nb_2O_5 (T-Nb_2O_5) was found to show the anomalously fast energy storage behavior (60 C rate) [5, 6], owing to its specific crystal structure. In the T-Nb_2O_5 crystal, loosely packed oxygen atomic layers and densely packed Nb–O atomic layers form a quasi-2D network for Li-ion incorporation, which allows direct Li-ion transport between bridging sites with very low steric hindrance [5]. Therefore, finding and designing electrode materials with specific atomic arrangements are still needed to obtain enhanced electrochemical properties [8, 9].

Niobium-based oxides, i.e., Nb_2O_5, $TiNb_xO_{2+2.5x}$ compounds, M–Nb–O (M = Cr, Ga, Fe, Zr, Mg, etc.) family, etc., showed fast charge storage performances because of their unique quasi-2D networks for Li-ion incorporation and both open and stable Wadsley–Roth shear crystal structures [10]. The finding and unraveling of new M–Nb–O materials systems are of great interest. Li–La–Nb–O and La–Nb–O compounds were served as solid-state electrolytes for the lithium-ion battery and fuel cell, which may show a fast Li-ion migration behavior. La–Nb–O compounds mainly contain La_3NbO_7, $LaNbO_4$, $LaNb_3O_9$, $LaNb_5O_{14}$, $La_2Nb_{12}O_{33}$, etc. [11, 12]. Most of niobium oxides consist of octahedral NbO_6 structures with different degree distortions, while the

✉ Dongfeng Xue
dongfeng@ciac.ac.cn

[1] State Key Laboratory of Rare Earth Resource Utilization, Changchun Institute of Applied Chemistry, Chinese Academy of Sciences, Changchun 130022, China

[2] Institute of Multidisciplinary Research for Advanced Materials, Tohoku University, Sendai 980-8577, Japan

tetrahedral NbO_4 structure only exists in the $LaNbO_4$ compound [13–15]. However, among niobium oxide compounds, the NbO_4 tetrahedron is rarely found, because the large Nb^{5+} atom cannot fit into the oxygen-anion tetrahedron. Electronegativity is a useful guideline tool to design targeted electrode materials [9]. With applying electronegativity of metal cations, the change of redox potential and the selectivity of targeted doping element can be achieved in the design of electrode materials [16–18]. Ionic electronegativity values of Nb^{5+} and La^{3+} are 1.862 and 1.327, respectively. In different La–Nb–O compounds, La^{3+} can decrease the orbital overlap by easing some charge densities of Nb–O bonds, leading to easy enable redox reaction of Nb^{5+}/Nb^{4+} and lithium-ion diffusion. With high electronegativity, tetrahedral NbO_4^{3-} species often do not exist in aqueous solution [19], except with the help of La^{3+}.

In this work, we synthesized orthorhombic pyrochlore $LaNb_5O_{14}$, perovskite $LaNb_3O_9$, and monoclinic $LaNbO_4$ compounds. In $LaNb_5O_{14}$, each Nb atom is surrounded by six or seven oxygen atoms to form a NbO_6 octahedron or tilted pentagonal bipyramids, while in $LaNb_3O_9$, each Nb atom forms a NbO_6 octahedron and 2/3 of La cation sites are vacant (Fig. 1). In the $LaNbO_4$ compound, a La cation is eightfold coordination and a Nb cation and 4 O anions form an NbO_4 tetrahedron. Served as electrode materials for lithium-ion batteries, the electrochemical performances of these La–Nb–O compounds were systematically studied.

2 Experimental

2.1 Material synthesis

La–Nb–O samples were synthesized with a one-step solid-state reaction. The stoichiometric amounts of Nb_2O_5 and La_2O_3 were weighed (Table 1) and milled in a mortar for 1 h. Then, the mixed powder was pressed into pellets under a pressure of 30 MPa and calcined in air at 1080 °C for 10 h. After that, the pellets were crushed and milled for further usage.

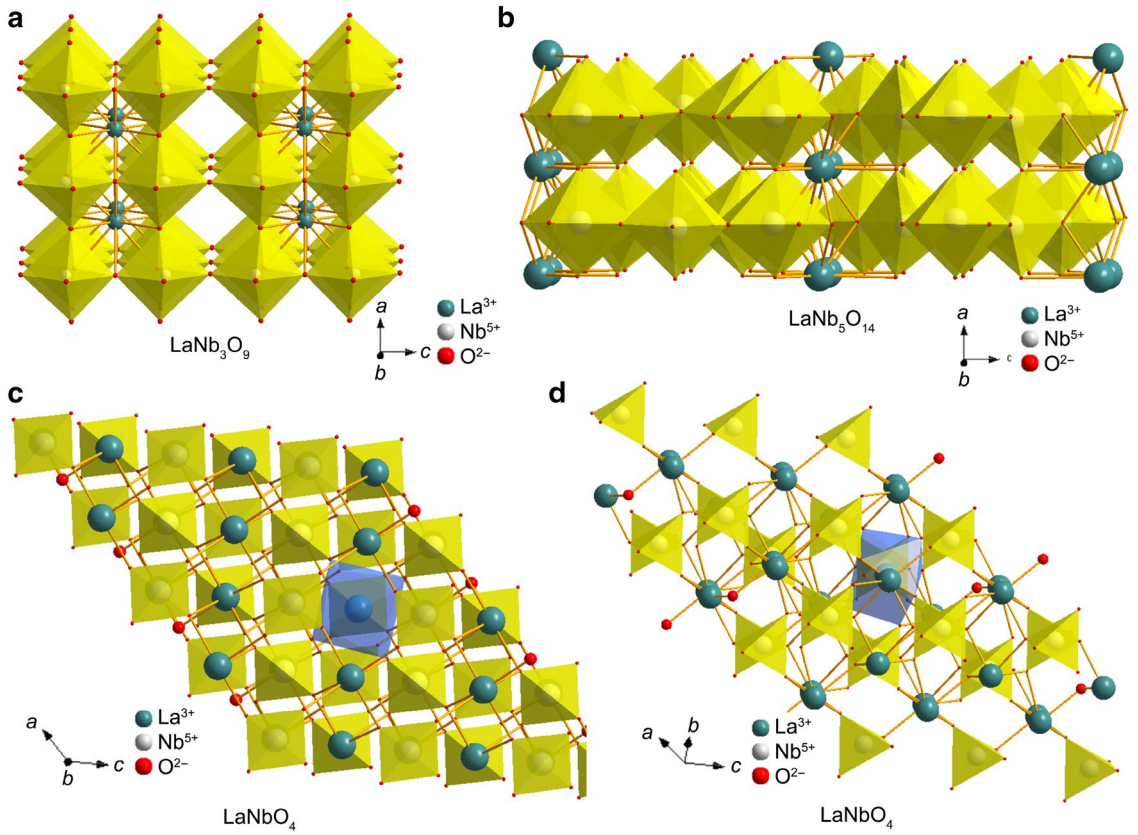

Fig. 1 Crystal structures of **a** $LaNb_3O_9$, **b** $LaNb_5O_{14}$, and **c**, **d** monoclinic $LaNbO_4$. $LaNb_3O_9$ includes octahedral NbO_6 and LaO_{12} structures. $LaNb_5O_{14}$ includes octahedral NbO_6, pentahedral NbO_7 and LaO_{12} structures. $LaNbO_4$ includes tetrahedrally coordinated NbO_4 and hexahedral LaO_8 units

Table 1 Experimental conditions of the as-synthesized samples and discharge capacitor

Sample	Atom ratio of Nb:La	Phase	First discharge capacity/ (mAh g^{-1})
1	7:1	$LaNb_5O_{14}+Nb_2O_5$	175
2	6:1	$LaNb_5O_{14}+Nb_2O_5$	160
3	5:1	$LaNb_5O_{14}$ + trace Nb_2O_5	116
4	4:1	$LaNb_5O_{14}$ + trace $LaNb_3O_9$	112
5	3:1	$LaNb_3O_9+LaNb_5O_{14}$	138
6	2:1	$LaNb_3O_9+LaNbO_4$ + trace $LaNb_5O_{14}$	122
7	1:1	$LaNbO_4$	60

2.2 Material characterization

The phase, image, and element mappings of La–Nb–O samples were analyzed by X-ray diffraction (XRD) with a D8 Focus X-ray diffractometer (Bruker) and field-emission scanning electron microscope (SEM, Hitachi S-4800). Raman spectra were measured in a Jobin–Yvon Horiba T64000 Raman triple grating spectrometer (Horiba Ltd., France) with a green line of Ar^+ laser (514.5 nm radiation).

2.3 Electrode preparation

The La–Nb–O sample was mixed with carbon black and polyvinylidene fluoride (PVDF) with a mass ratio of 70:15:15 to form slurry and coated on an Al foil, which was served as the cathode. The assembled half-cells used lithium metal as the anode. The cathode and anode were assembled into a CR2032 coin cell in an Ar-filled glovebox. The separator is a polypropylene film (Celgard 2400) and the electrolyte is 1 mol L^{-1} $LiPF_6$ in ethylene carbonate/dimethyl carbonate/diethyl carbonate (EC/DMC/DEC, 1:1:1 vol%).

2.4 Electrochemical measurement

A charge–discharge cycling test of the assembled half-cell was performed on a LAND CT2001A system in the voltage range of 1.0–3.0 V (vs. Li^+/Li) at different current densities. Cyclic voltammogram (CV) curves were measured at an electrochemical workstation (CHI 660E).

3 Results and discussion

Different La–Nb–O compounds were synthesized by solid-state reaction. Figure 2 show XRD patterns of as-synthesized La–Nb–O compounds. When the atom ratios

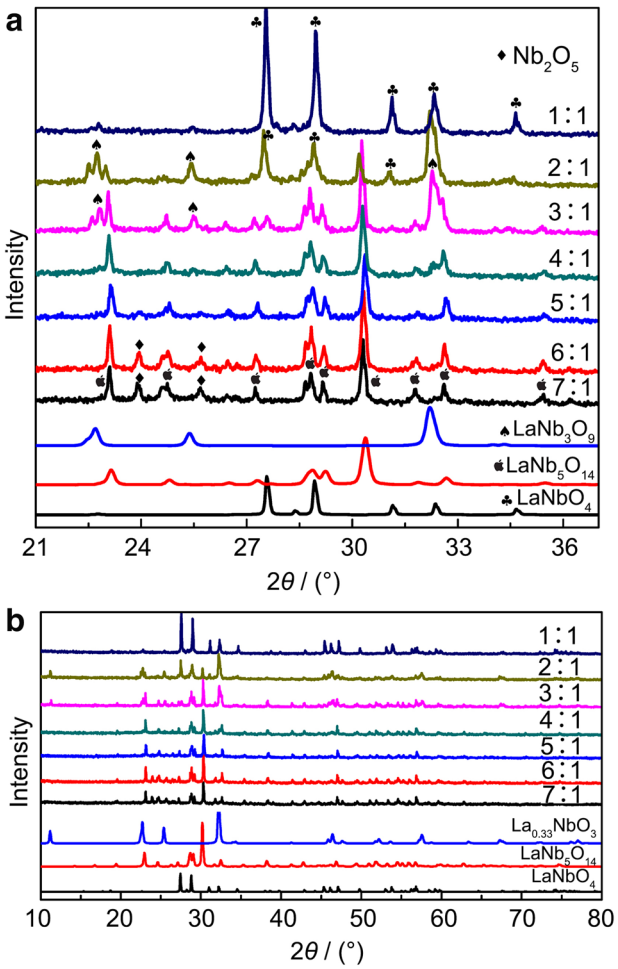

Fig. 2 **a**, **b** XRD patterns of La–Nb–O compounds with different atom ratios of Nb:La (JCPDS No. 76-263 for $LaNb_5O_{14}$, JCPDS No. 72-1121 for monoclinic Nb_2O_5, JCPDS No. 72-2080 for $LaNb_3O_9$, and JCPDS No. 22-1125 for monoclinic $LaNbO_4$)

of Nb:La vary from 7:1 to 4:1, the main phase of samples is orthorhombic pyrochlore $LaNb_5O_{14}$ (JCPDS No. 76-263) with the trace phase of monoclinic Nb_2O_5 (JCPDS No. 72-1121). Orthorhombic pyrochlore $LaNb_5O_{14}$ is constituted by corner and edge-sharing NbO_6 and NbO_7 polyhedra, which also includes loosely packed La–O atomic layers and densely packed Nb–O atomic layers, forming a quasi-2D network for Li-ion insertion (Fig. 1b). When the atom ratios of Nb:La are between 3:1 and 2:1, the main phase of samples is orthorhombic perovskite $LaNb_3O_9$ (JCPDS No. 72-2080) with the trace phase of monoclinic $LaNbO_4$. Pure phase monoclinic $LaNbO_4$ (JCPDS No. 22-1125) was obtained at the atom ratio 1:1 of Nb:La. Monoclinic $LaNbO_4$ includes isolated NbO_4 tetrahedra which are interlinked by eightfold coordination LaO_8 (Fig. 1c, d). SEM shows that the as-obtained samples have large particles with several micrometer and uniform distribution of La, Nb, and O elements (Fig. 3).

Raman spectroscopy is a powerful tool for probing chemical and structural properties of La–Nb–O materials. As shown in Fig. 4, the band in the range of 450–850 cm^{-1} can be assigned to the Nb–O-stretching modes. The O–Nb–O-bending modes appear below 450 cm^{-1}, which are strongly interacted with the O–La–O-bending and La–O-stretching modes [19, 20]. The 670 cm^{-1} band originates from the symmetric stretching mode of NbO_6 octahedra (Fig. 4d). Both $LaNb_5O_{14}$ and $LaNb_3O_9$ compounds include the NbO_6 octahedral structure with different degree distortions. Therefore, $LaNb_5O_{14}$ and $LaNb_3O_9$ compounds show similar Raman bands. However, only the NbO_4 tetrahedral structure exists in the $LaNbO_4$ compound. The Raman bands centered at 810 and 320 cm^{-1} are due to the Nb–O symmetric modes of NbO_4 tetrahedral structure.

Electrochemical performances of La–Nb–O compounds were further studied as electrode materials for lithium-ion batteries. CV was used to demonstrate their electrochemical reaction mechanisms. Figure 5 shows CV curves of La-Nb–O compounds with different atom ratios of Nb:La at scan rate of 0.5 mV s^{-1} and potential range of 1.0–3.0 V. These La–Nb–O electrodes have high working voltages of > 1.0 V, which can suppress the formation of the solid electrolyte interface film and lithium dendrites, ensuring the safety of working batteries [10]. When the atom ratios of Nb:La were changed from 7:1 to 5:1, one couple of main redox peaks centered at 1.59 and 1.77 V and weak redox peaks of 2.05/1.90 V were appeared. The redox peaks are assigned to the redox reaction of Nb^{5+}/Nb^{4+} couple in different chemical environments of NbO_6 and NbO_7 [21].

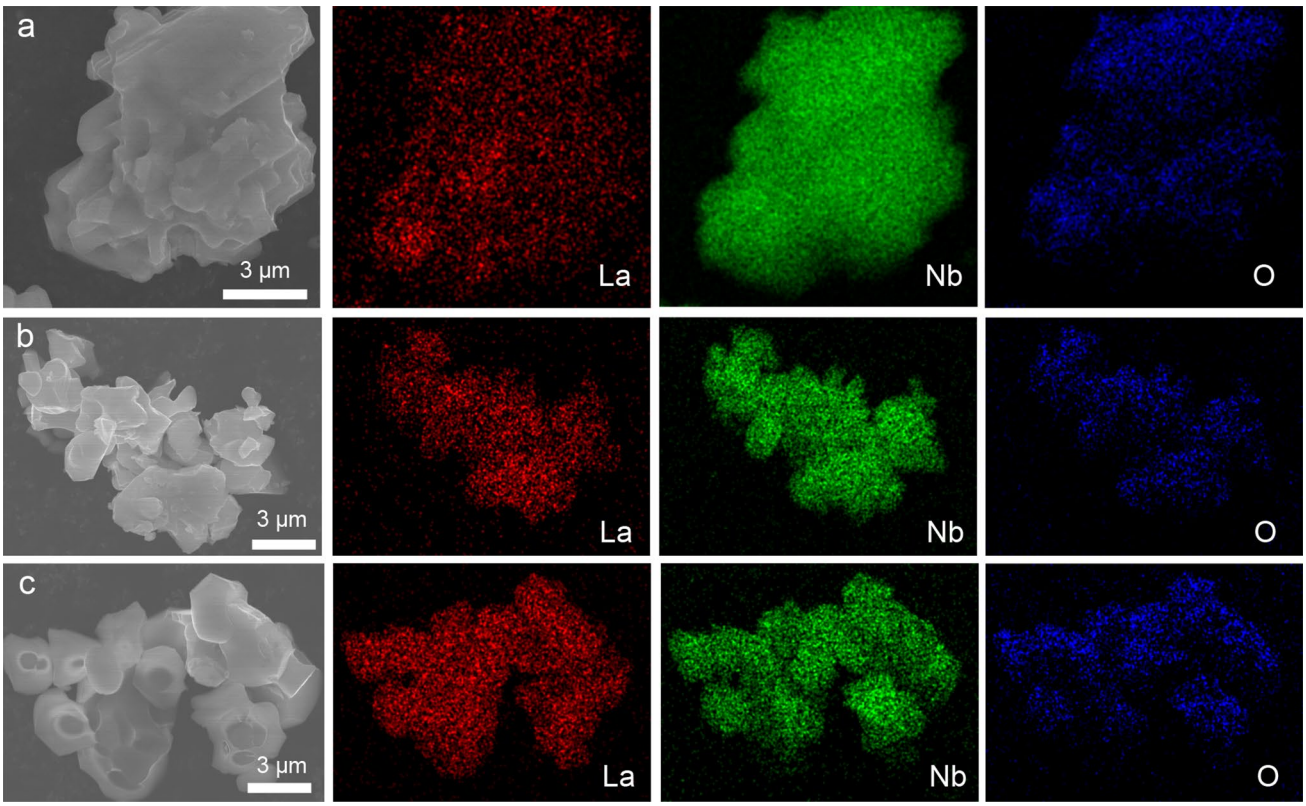

Fig. 3 SEM images and element mapping of **a** 1# sample (the atom ratio of Nb:La is 7:1), **b** 5# sample (the atom ratio of Nb:La is 3:1), and **c** 7# sample (the atom ratio of Nb:La is 1:1)

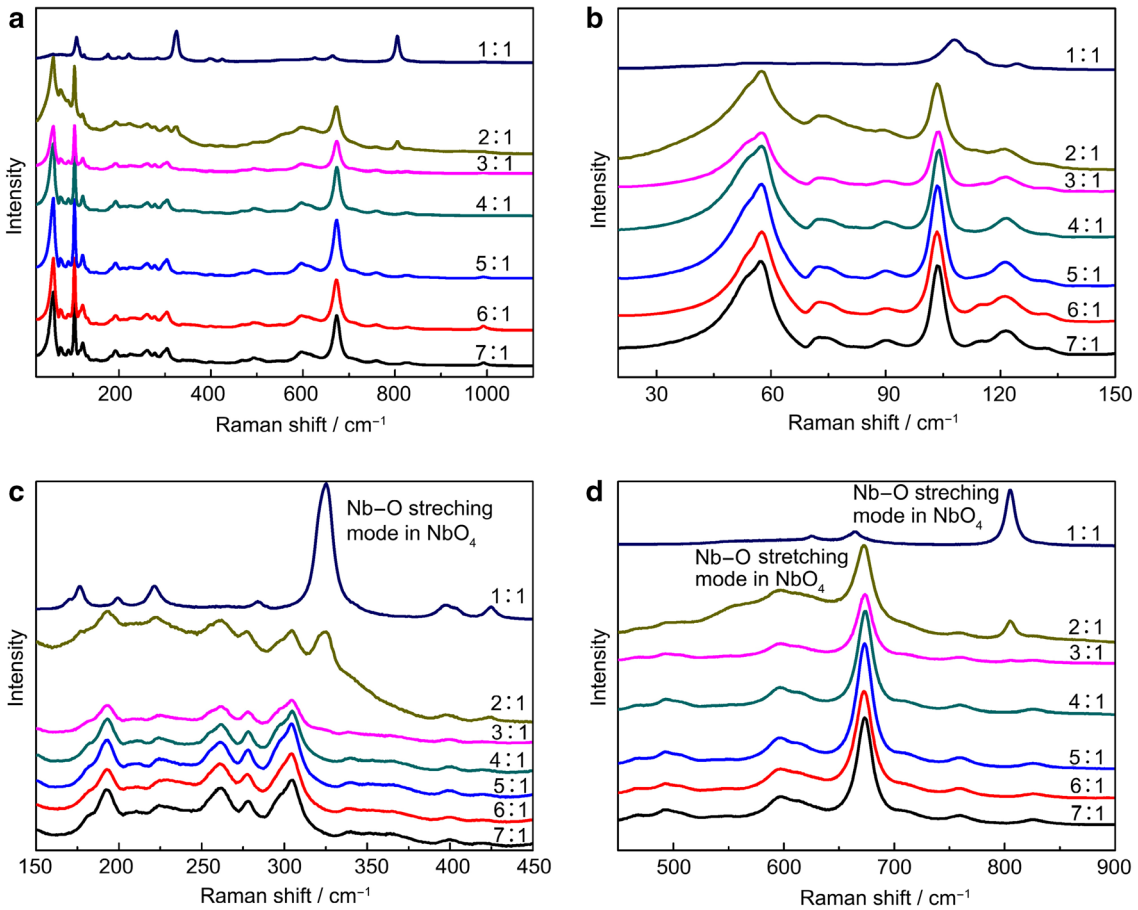

Fig. 4 **a** Raman spectra of La–Nb–O compounds with different atom ratios of Nb:La; **b–d** Enlarged Raman spectra of La–Nb–O compounds with different atom ratios of Nb:La

Beginning from 4:1 of the Nb:La atom ratio, positions of main redox peaks were changed to 1.16 and 1.29 V, while the intensity of redox peaks of 1.59 and 1.77 V decreased. Only NbO_6 and NbO_4 exist in $LaNb_3O_9$ and $LaNbO_4$, respectively. The above results show that rare earth La^{3+} can change the thermodynamic potential of Nb^{5+}/Nb^{4+} redox reaction by changing the crystal structure and Nb coordination condition.

Furthermore, we studied the charge–discharge performances of these La–Nb–O compounds. The first discharge capacities at the current density of 100 mA g^{-1} are 175, 160, 116, 112, 138, 122, and 60 mAh g^{-1} for different samples (Table 1, Fig. 6 and 7). The La–Nb–O compound with the Nb:La atom ratio of 7:1 shows the highest capacity among 1–7# La–Nb–O compounds. The capacity contribution originates from Nb^{5+}/Nb^{4+} redox reaction coupled with lithium-ion intercalation. Thus, $LaNb_5O_{14}$ with a quasi-2D network structure can favor the insertion of Li-ion (Fig. 1b) to obtain a high capacity. The rate capability was tested at various current densities from 0.1 to 2 A g^{-1} (Fig. 6a). The La–Nb–O compound with the Nb:La atom ratio of 2:1 exhibits a higher capacity especially at a discharge rate of 2 A g^{-1} than that of 1–5# and 7# La–Nb–O compounds. The NbO_6 framework structure and many La vacant sites in $LaNb_3O_9$ provide a stable host for fast lithium intercalation. Owing to high electronegativity of tetrahedral NbO_4^{3-} species in $LaNbO_4$, this compound only displays the smallest capacity and bad rate performance than that of 1–6# La–Nb–O compounds [19, 22]. Electrochemical impedance spectra are used to analyze the resistance during electrochemical reaction. Figure 6d shows Nyquist plots of as-synthesized La–Nb–O compounds. The calculated charge transfer resistances of most La–Nb–O compounds have small values of $< 50\ \Omega$, which indicate that La–Nb–O electrodes have low resistances.

To study the fast rate performance, we studied the charge storage kinetics of La–Nb–O compounds using CV curves at

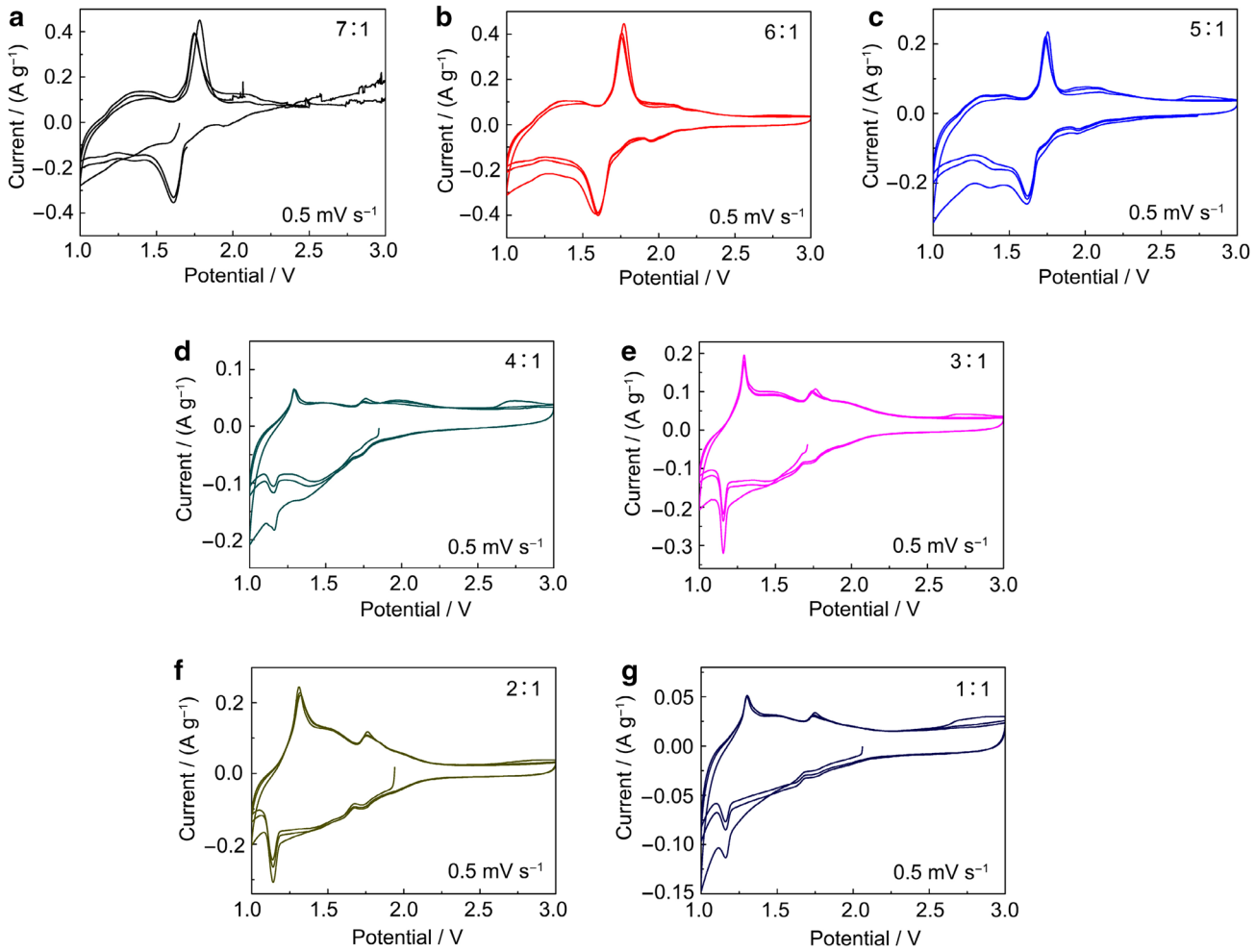

Fig. 5 CV curves of La–Nb–O compounds with different atom ratios of Nb:La at a scan rate of 0.5 mV/s and a potential range of 1–3 V

different scan rates. The relationship of the peak current and scan rate satisfies the following equation [23, 24]:

$$i = av^b, \tag{1}$$

where $b = 0.5$ indicates that the electrochemical reaction is controlled by a semi-infinite diffusion process, whilst $b = 1$ indicates a capacitive behavior. The b values for the La–Nb–O compounds are between 0.6 and 0.8, indicating a hybrid diffusion and capacitive processes (Fig. 6e, f) [25, 26]. The above results show that La–Nb–O compounds with specific crystal structures can provide the lithium diffusion pathway for fast lithium intercalation reaction. The design of novel complex compounds with targeted performance needs the control of the crystal structure and ionic electronegativity of component elements [27].

To study the energy storage mechanism of these electrode materials, XRD and Raman analyses were used to measure the electrode after electrochemical reaction (Fig. 8). $LaNb_5O_{14}$, $LaNb_3O_9$, and $LaNbO_4$ phases are not changed after lithium insertion reaction (Fig. 8a). The existence of the peak at 805 cm^{-1} indicates the retaining of the NbO_4 structure in the $LaNbO_4$ compound. Raman peaks of La–Nb–O compounds with Nb:La atomic ratios of 7:1 and 3:1 are at 649 and 647 cm^{-1}, which are consistent with Nb–O-stretching vibration of NbO_6 or NbO_7 structures [19, 20]. The results show that the La–Nb–O compound is an intercalation-type material for lithium storage.

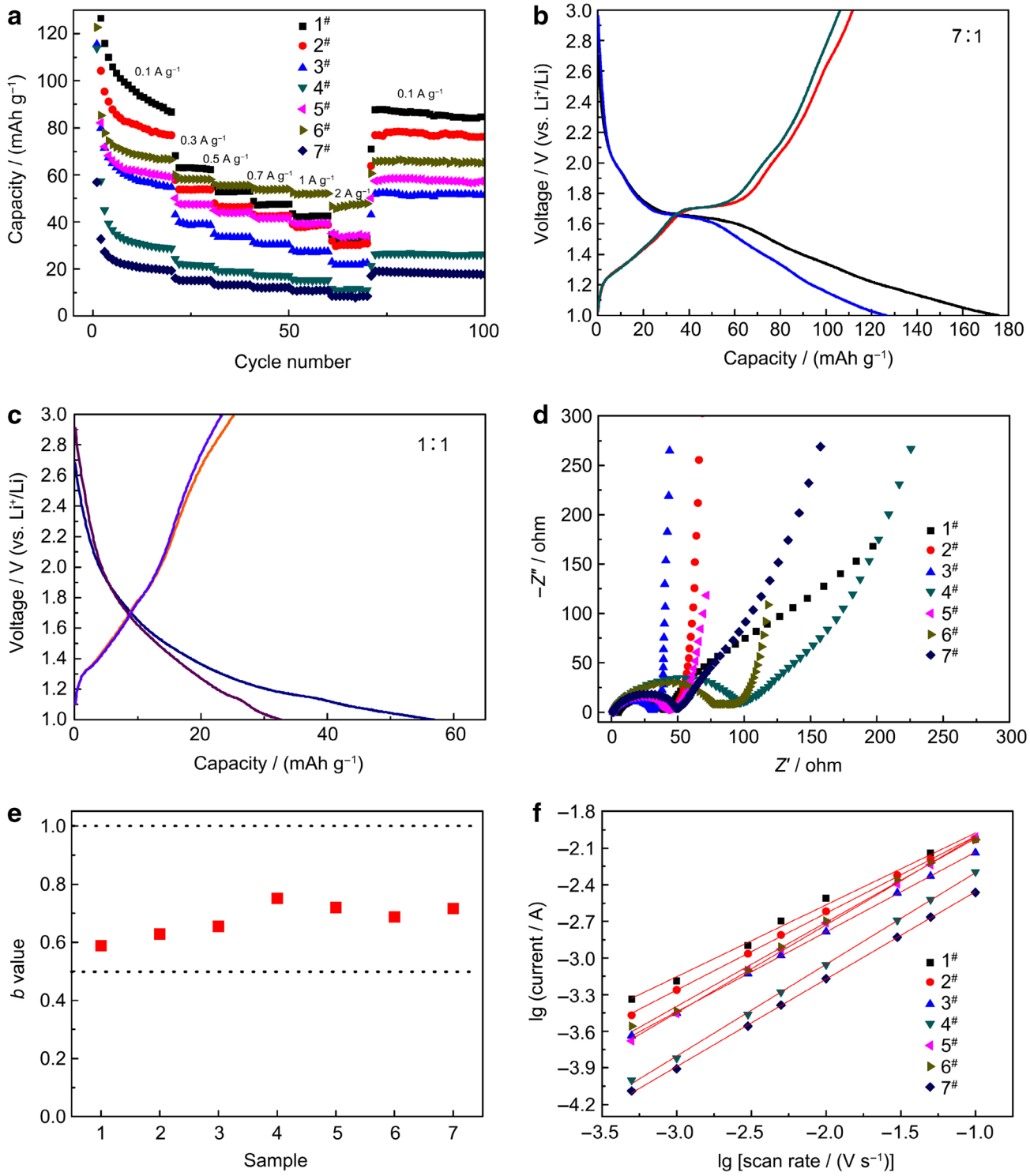

Fig. 6 Electrochemical performances of La–Nb–O compounds with different atom ratios of Nb:La. **a** Rate performance of 1#-7# La–Nb–O compounds; **b**, **c** charge–discharge curves of 1# and 7# samples, respectively; **d**–**f** EIS curves, *b* values, and lg (current) vs. lg (scan rate) of 1#–7# La–Nb–O compounds

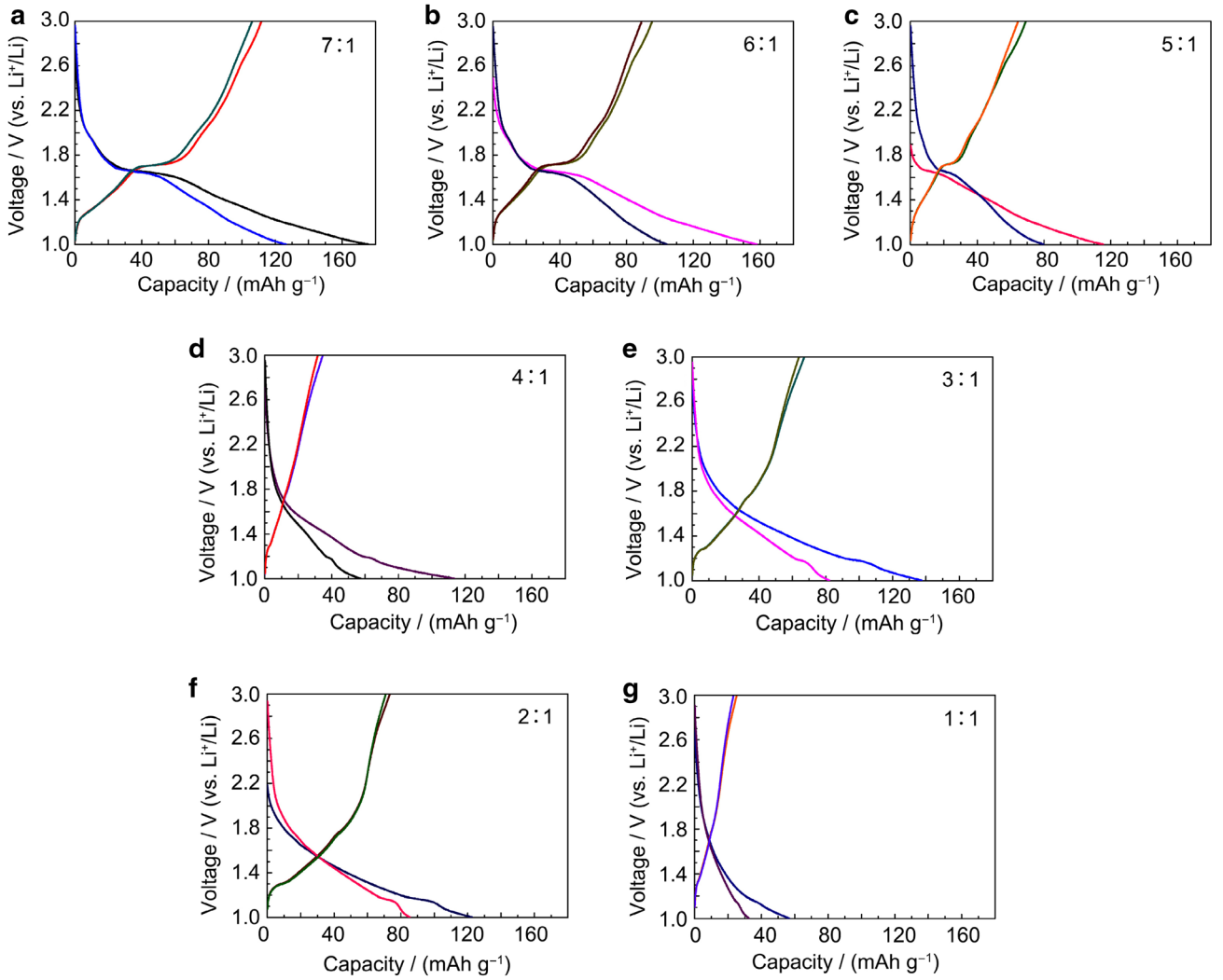

Fig. 7 Charge–discharge curves of La–Nb–O compounds with different Nb:La atom ratios

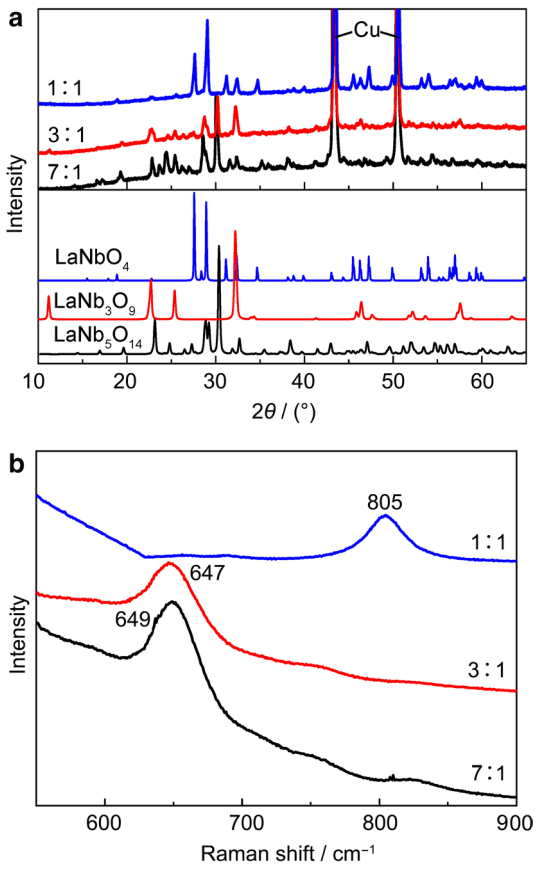

Fig. 8 **a** XRD patterns and **b** Raman spectra of La–Nb–O compounds after lithium-ion insertion with different atom ratios of Nb:La

4 Conclusion

In conclusion, orthorhombic pyrochlore $LaNb_5O_{14}$, perovskite $LaNb_3O_9$, and monoclinic $LaNbO_4$ compounds were obtained among La–Nb–O compounds. Pyrochlore $LaNb_5O_{14}$ showed the highest discharge capacities of 175 mAh g^{-1} at the current density of 100 mA g^{-1}, when used as cathode materials for fast lithium-ion energy storage. Perovskite $LaNb_3O_9$ displayed the highest discharge capacities of 51 mAh g^{-1} at current density of 2 A g^{-1}. In both $LaNb_5O_{14}$ and $LaNb_3O_9$, La cation is 12-fold coordination and Nb cations form a sixfold and sevenfold coordination polyhedra, which construct the quasi-2D lithium-ion diffusion network. $LaNbO_4$ with a NbO_4 tetrahedral structure showed bad electrochemical performances. The results showed that the enhanced performances of cathode materials originated from appropriate three-dimensional oxide crystal structures, which might be identified and selected through ionic electronegativity scale.

Acknowledgements This work was financially supported by the National Natural Science Foundation of China (Grant No. 21601176), CAS-VPST Silk Road Science Found 2018 (Grant No. GJHZ1854), the Youth Innovation Promotion Association, CAS (Grant No. 2018262), Jilin Province Youth Talent Lifting Project (Grant No. 181901), and the Youth Talent Development Program of the State Key Laboratory of Rare Earth Resource Utilization (Grant No. RERUY2017004).

References

1. Harada JK, Charles N, Poeppelmeier KR, Rondinelli JM. Heteroanionic materials by design: progress toward targeted properties. Adv Mater. 2019;31(19):1805295.
2. Freire M, Kosova NV, Jordy C, Chateigner D, Lebedev OI, Maignan A, Pralong V. A new active Li–Mn–O compound for high energy density Li-ion batteries. Nat Mater. 2016;15:173.
3. Chen K, Song S, Liu F, Xue D. Structural design of graphene for use in electrochemical energy storage devices. Chem Soc Rev. 2015;44(17):6230.
4. Griffith KJ, Wiaderek KM, Cibin G, Marbella LE, Grey CP. Niobium tungsten oxides for high-rate lithium-ion energy storage. Nature. 2018;559:556.
5. Chen D, Wang JH, Chou TF, Zhao B, El-Sayed MA, Liu M. Unraveling the nature of anomalously fast energy storage in T-Nb2O5. J Am Chem Soc. 2017;139(20):7071.
6. Griffith KJ, Forse AC, Griffin JM, Grey CP. High-rate intercalation without nanostructuring in metastable Nb_2O_5 bronze phases. J Am Chem Soc. 2016;138(28):8888.
7. Odziomek M, Chaput F, Rutkowska A, Świerczek K, Olszewska D, Sitarz M, Lerouge F, Parola S. Hierarchically structured lithium titanate for ultrafast charging in long-life high capacity batteries. Nat Commun. 2017;8:15636.
8. Chen K, Xue D. Crystallization of transition metal oxides within 12 seconds. Cryst Eng Comm. 2017;19:1230.
9. Chen K, Xue D. Materials chemistry toward electrochemical energy storage. J Mater Chem A. 2016;4(20):7522.
10. Deng Q, Fu Y, Zhu C, Yu Y. Niobium-based oxides toward advanced electrochemical energy storage: recent advances and challenges. Small. 2019;15(32):1804884.
11. Miruszewski T, Winiarz P, Dzierzgowski K, Wiciak K, Zagórski K, Morawski A, Mielewczyk-Gryń A, Wachowski S, Strychalska-Nowak J, Sawczak M, Gazd M. Synthesis, microstructure and electrical properties of nanocrystalline calcium doped lanthanum orthoniobate. J Solid State Chem. 2019;270:601.
12. Wachowski S, Mielewczyk-Gryn A, Zagorski K, Li C, Jasinski P, Skinner SJ, Haugsrud R, Gazda M. Influence of Sb-substitution on ionic transport in lanthanum orthoniobates. J Mater Chem A. 2016;4:11696.
13. Brunckova H, Medvecky L, Kovalcikova A, Fides M, Mudra E, Durisin J, Sebek M, Kanuchova M, Skvarla J. Structural and mechanical properties of $La_{1/3}NbO_3$ and $La_{1/3}TaO_3$ thin films prepared by chemical solution deposition. J Rare Earths. 2017;35(11):1115.
14. Brunckova H, Medvecky L, Hvizdos P, Girman V. Effect of solvent on phase composition and particle morphology of lanthanum niobates prepared by polymeric complex sol–gel method. J Sol Gel Sci Technol. 2014;69(2):272.
15. Brunckova H, Medvecky L, Hvizdos P, Durisin J, Girman V. Structural and mechanical properties of sol–gel prepared pyrochlore lanthanum niobates. J Mater Sci. 2015;50(22):7197.
16. Li K, Shao J, Xue D. Site selectivity in doped polyanion cathode materials for Li-ion batteries. Funct Mater Lett. 2013;6(4):1350043.
17. Li K, Xue D. Estimation of electronegativity values of elements in different valence states. J Phys Chem A. 2006;110(39):11332.

18. Melot BC, Tarascon JM. Design and preparation of materials for advanced electrochemical storage. Acc Chem Res. 2013;46(5):1226.
19. Jehng JM, Wachs IE. Structural chemistry and Raman spectra of niobium oxides. Chem Mater. 1991;3(1):100.
20. Ishii K, Morita N, Nakayama K, Tsunekawa S, Fukuda T. Raman spectra of $LaNbO_4$ in the ferroelastic phase and the relaxation after the state shift. Phys Status Solidi A. 1989;112(1):207.
21. Griffith KJ, Senyshyn A, Grey CP. Structural stability from crystallographic shear in TiO_2–Nb_2O_5 phases: cation ordering and lithiation behavior of $TiNb_{24}O_{62}$. Inorg Chem. 2017;56(7):4002.
22. Cao Y, Duan N, Yan D, Chi B, Pu J, Jian L. Enhanced electrical conductivity of $LaNbO_4$ by A-site substitution. Int J Hydrogen Energy. 2016;41(45):20633.
23. Deng T, Zhang W, Arcelus O, Kim JG, Carrasco J, Yoo SJ, Zheng W, Wang J, Tian H, Zhang H, Cui X, Rojo T. Atomic-level energy storage mechanism of cobalt hydroxide electrode for pseudocapacitors. Nat Commun. 2017;8:15194.
24. Chen K, Xue D. How to high-efficiently utilize electrode materials in supercapattery? Funct Mater Lett. 2019;12(1):1830005.
25. Lukatskaya MR, Kota S, Lin Z, Zhao MQ, Shpigel N, Levi MD, Halim J, Taberna PL, Barsoum MW, Simon P, Gogotsi Y. Ultra-high-rate pseudocapacitive energy storage in two-dimensional transition metal carbides. Nat Energy. 2017;2:17105.
26. Liang X, Chen K, Xue D. A flexible and ultrahigh energy density capacitor via enhancing surface/interface of carbon cloth supported colloids. Adv Energy Mater. 2018;8(16):1703329.
27. Sun C, Xue D. Multisize and multiweight effects in materials science and engineering. Sci China Technol Sci. 2019;62(4):707.

Prof. Dongfeng Xue, FRSC, received his PhD from Changchun Institute of Applied Chemistry, Chinese Academy of Sciences (CIAC, CAS) in 1998. From 1999 to 2003, he worked at the Universitaet Osnabrueck (AvH research fellow), the University of Ottawa (postdoctoral researcher), and the National Institute for Materials Science, Japan (JSPS postdoctoral researcher). In 2001, he was appointed as a full professor at Dalian University of Technology. In 2011, he joined CIAC as a full professor. Since 2018, he has served as the associate editor of *CrystEngComm*. His research interests focus on multiscale crystallization of inorganic matter for energy and optical applications.